Journal of Engineering Science and Technology
Vol. 11, No. 6 (2016) 768 - 787

EFFECT OF END ANCHORAGE LENGTH AND STIRRUP RATIO ON BOND AND SHEAR CAPACITY OF CONCRETE BEAMS WITH NONMETALLIC REINFORCEMENT

RENDY THAMRIN

Department of Civil Engineering, Faculty of Engineering, Andalas University,
Padang, 25163, West Sumatera, Indonesia
E-mail: rendy@ft.unand.ac.id

Abstract

This paper presents a study on the effect of end anchorage length and stirrup ratio on bond and shear capacity of concrete beams reinforced with Carbon Fiber Reinforced Polymer (CFRP) bars. This study was carried out using test data on nine simply supported reinforced concrete beams with stirrups. The beams were subjected to two point monotonic loads and the test variables were the length of end anchorage and the stirrup ratio. Theoretical equations for calculating bond strength and shear capacity obtained from literature were applied and then compared with experimental values. Beams with inadequate end anchorage length showed premature bond failure even when there was sufficient stirrup ratio. Beams with adequate end anchorage length failed in shear or flexure modes depending on the stirrup ratio. A numerical model for bond stress and slip in response to pullout forces was also used to determine analytically the bond stress distributions along end anchorage. The behavior of tensile force acting on the stirrups was also examined. Finally, a simple model for predicting tension force acting on the stirrups was proposed.

Keywords: bond and shear capacity, reinforced concrete beams, CFRP bar, end anchorage length, stirrup ratio.

1. Introduction

Shear failure in reinforced concrete beams is principally indicated by propagation of diagonal shear cracks in the shear span zone. The occurrence of diagonal shear crack affects the distribution of tensile force along the longitudinal reinforcement and a significant quantity of tensile force develops at the support [1-3]. In his extensive report, Mylrea [4] suggested that extending the bar past the support may

Nomenclatures

A_c	Area of concrete rectangular prism
A_f	Area of longitudinal reinforcement
A_v	Area of shear reinforcement
a	Shear span length
b	Width of web
b_i	Parameter for geometrical arrangement of main bars
c	Neutral axis depth
c_b	Cover concrete
d	Effective depth
d_b	Diameter of longitudinal bar
E_c	Modulus elasticity of concrete
E_f	Modulus elasticity of CFRP bar
E_s	Modulus elasticity of steel bar
f_c'	Concrete compressive strength
f_u	Tensile strength of CFRP bar
f_y	Yield strength of steel bar
f_{ys}	Yield strength of steel stirrups
k	$(1+\sqrt{(200/d)}) \leq 2.0$
k_{FM}	Coefficient representing the efficiency of stirrups
L_a	End anchorage length
n	Ratio of modulus elasticity (E_f/E_c)
N	Number of longitudinal reinforcement
N_s	Number of stirrups along the shear span zone
P_c	Force in concrete segment of concrete rectangular prism
P_f	Force in reinforcement
V_c	Shear capacity of concrete
V_s	Shear capacity provided by stirrup
V_{bond}	Shear capacity calculated from bond capacity
$V_{flex.}$	Shear capacity calculated from flexural capacity
V_{shear}	Shear capacities
S_x	Local slip
s	Spacing of stirrups
T	Tensile force on longitudinal reinforcement
T_s	Tensile force on stirrups
T_{sy}	Tensile force on stirrups at yield

Greek Symbols

ε	Measured strain of longitudinal reinforcement
ε_c	Strain of concrete
ε_f	Strain of reinforcement
ϕ	Perimeter of reinforcement
ρ	Ratio of longitudinal reinforcement and concrete prism area (A_f/A_c)
ρ_w	Ratio of longitudinal reinforcement in tension
ρ_s	Stirrup ratio
τ	Local bond stress
τ_{co}	Bond strength without stirrups
τ_{max}	Maximum bond stress
τ_{st}	Additional bond strength due to stirrups
τ_u	Total bond strength
ω	Parameter for tensile force equation of stirrups

Abbreviations

CFRP	Carbon Fiber Reinforced Polymer
LVDT	Linear Variable Differential Transformer

result in a better tensile force distribution and provide higher bond capacity. Pay et al. [5] recently report that flexural bond strength is affected by modulus elasticity and axial rigidity of longitudinal reinforcement. It is also confirmed in their report that the bond length in splice region affects bond strength. The test result clarified by Pay et al. supports the previous report described by Mylrea [4] concerning the requirement of bond length of tensile reinforcement.

Meanwhile, a series of experimental studies on shear capacity of concrete beams with stirrups and longitudinally reinforced with Glass Fiber Reinforced Polymer (GFRP) bars were carried out by Azlina et al. [6-8]. These studies confirm that a significant amount of tensile force exists at the support region due to the occurrence of the diagonal shear cracks. This suggests that longitudinal reinforcement in the shear span zone must be sufficiently extended into the support to avoid bond-splitting failure due to some shifting of the tensile force. ACI 318-08 [9] requires that the reinforcement shall extend into the support (L_a) at least 150 mm to provide end anchorage (see Fig. 1). Alternatively, end hook shape can be used as anchorage. This method is the most commonly used in reinforced concrete structures with steel bars.

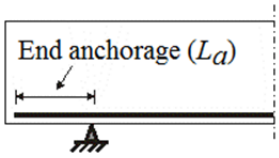

Fig. 1. End anchorage of tensile reinforcement in the support region (La) [9].

However, it is not possible to bend the nonmetallic reinforcements (GFRP, and CFRP) on site owing to the inflexibility of the bar [10]. Consequently, careful attention should be paid regarding the design of the end anchorage length in the support region. On the other hand, as yet, no information can be found from ACI 440.1R-06 related to the provision of end anchorage length of FRP reinforcement. For this reason, a model for predicting the tension force at the support due to the occurrence of diagonal shear cracks and shifting of the tensile force was proposed by author [11] in a previous study.

Effect of stirrups on bond strength has been investigated in earlier studies by other researchers over the last five decades [12, 13]. Morita and Fujii [12] clarified that the number of stirrups plays a significant role on bond failure mode after the splitting of the surrounding concrete. In their report, they proposed an empirical equation for predicting the anchorage bond strength. In another report, Plizzari et al. [13] described the relationship between the anchorage capacity and the quantity of stirrups by introducing a parameter called stirrup index of confinement. They have observed that anchorage capacity increases as the stirrup index of confinement increases up to an upper bound. However, it is the concern of the author that the number of experimental studies investigating the behavior of steel stirrups in concrete beams reinforced with GFRP bars with short shear spans (a/d < 2.5) is still inadequate. Therefore, the main purpose of this paper is to respond to this lack by focusing on bond stress behavior of end anchorage at the support region and the tensile forces acting on the stirrups.

In this investigation the author's test data [3] on nine concrete beams was analysed to examine the effect of end anchorage length and the effect of stirrup ratio on beam capacity. Bond strength of the beams calculated using empirical equation is compared to that obtained from the test data. Numerical analysis was also carried out to predict the distribution of bond stresses along the end anchorage. In addition, the behavior of tensile force acting on the stirrups was examined. Finally, a simple empirical model for predicting the growth of tensile force acting on the stirrups after the occurrence of diagonal shear crack was developed from the data.

2. Experimental Study

2.1. Beam specimens and materials

The author's test data [3] on nine simply supported reinforced concrete beam monotonically subjected to two point load were used. The beam size was 130 mm wide, 230 mm deep, and 1300 mm span length. All of the beams were longitudinally reinforced (tensile reinforcement) with deformed CFRP bars. CFRP bars used in this study were produced by Fukui Fibertech, Co. Ltd. Japan and contain of 60% carbon fiber. The tensile strength, f_u, of CFRP bars was about 1800 MPa with modulus elasticity, E_f, of 160 GPa. The longitudinal compression reinforcement was deformed steel bars with 10 mm diameter, yield strength, f_y, of 403 MPa, and a modulus elasticity, E_s, of 168 GPa. Figure 2 shows steel and GFRP bars used in this study (the unit shown is in mm). The stirrups used were closed type with 6 mm diameter and yield strength, f_{ys}, of 823 MPa. Additionally, the concrete compressive strength, f_c', at age 28 days was 38.4 MPa.

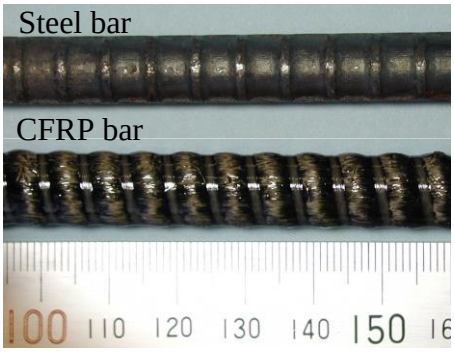

Fig. 2. CFRP and steel bars used in this study.

2.2. Beam test set-up

The main test variables used were end anchorage length beyond the support and stirrup ratio. In order to obtain the strain distribution of tensile longitudinal reinforcement, strain gages were placed at the support, at the middle point of shear span, and at the loading point. Strain gages (identified as S1 until S10) were also attached on stirrups as illustrated in Fig. 3. Deflections of the beam were measured using three Linier Variable Differential Transformers (LVDT) placed at midspan and at loading points (see Fig. 3).

Effect of end anchorage length on the bond stresses was investigated using three different bond lengths (L_a), i.e., 25 mm, 105 mm, and 210 mm, measured from the support as shown in Fig. 3. Plastic pipes were used to eliminate bond between concrete and reinforcement as shown in Fig. 3. The effect of stirrups on the shear span was examined using three different reinforcement ratios, ρ_s, as listed in Table 2, i.e., 0.48%, 0.72%, and 1.09%.

The beam was subjected to two point loads 400 mm apart. In order to ensure the occurrence of diagonal shear cracks and resulting tension shift, all of the beams were designed with 450 mm shear span length as shown in Fig. 3, hence the ratio of shear span to effective depth is smaller than 2.5.

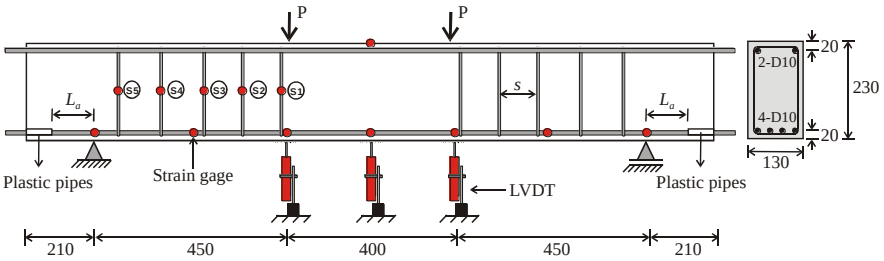

Fig. 3. Beam dimension, position of loads, LVDT's, and strain gages.

3. Shear and Bond Strength

3.1. Shear strength

For all of the beams, the shear capacity provided by concrete, V_c, was estimated theoretically using five equations obtained from literature and design codes listed in Table 1. Equations (1) and (2) were used as representative of empirical equations proposed by other researchers [14, 15], while Eq's (3), (4), and (5) were used as representative of the international codes for concrete structures reinforced with steel and FRP bars [16, 9, 10].

Table 1. Theoretical equations for shear capacity of concrete.

References	Equations for shear capacity of concrete	
Zsutty [14]	$V_c = 2.17[\rho_w f_c^{'}(d/a)]^{1/3} bd$	(1)
Niwa et al. [15]	$V_c = 0.2(\rho_w f_c^{'})^{1/3}(d^{-1/4})[0.75 + 1.4(d/a)]\, bd$	(2)
Eurocode 2 [16]	$V_c = [0.12k(100\rho_w f_c)^{1/3}]bd$	(3)
ACI 318-08 [9]	$V_c = [0.16\sqrt{f_c^{'}} + 17\rho_w(d/a)]\, bd$	(4)
ACI 440.1R-06 [10]	$V_c = (2/5)\sqrt{f_c^{'}} bc$	(5)

Shear capacities provided by stirrups, V_s, were calculated using equation provided by ACI 318-08 as written in Eq. (6):

$$V_s = \frac{A_v f_{ys} d}{s} \tag{6}$$

where A_v is the area of shear reinforcement, f_{ys} is the yield strength of stirrups, d is the effective depth, and s is the spacing of stirrups.

3.2. Bond strength

Experimental bond stresses, $\tau_{exp.}$, at the end anchorage at support region were calculated using Eq. (7):

$$\tau_{\text{exp.}} = \frac{T_{\text{exp.}}}{L_a \phi} = \frac{\varepsilon E_f A_f}{L_a \phi} \tag{7}$$

where T is the tensile force at the support, ε is the measured strain of longitudinal reinforcement at the support, E_f is the elastic modulus of CFRP, A_f is the area of longitudinal reinforcement, L_a is the end anchorage length beyond the support region, and ϕ is the perimeter of CFRP bar.

Furthermore, the following equation proposed by Morita and Fujii [12] was used to evaluate bond strength theoretically:

$$\tau_u = \tau_{co} + \tau_{st} \tag{8}$$

where:

$$\tau_{co} = (0.117 b_i + 0.163)\sqrt{f_c'} \tag{9}$$

$$\tau_{st} = (9.51 \frac{k_{FM} A_{st}}{s N d_b})\sqrt{f_c'} \tag{10}$$

where τ_u is the total bond strength, τ_{co} is the bond strength without stirrups, b_i is the parameter for evaluating the geometrical arrangement of longitudinal bars, f'_c is the concrete compression strength, τ_{st} is the additional bond strength due to stirrups, k_{FM} is the coefficient representing the efficiency of stirrups (in this study $k_{FM} = \sqrt{2}$); A_{st} is the total area of stirrup leg, s is the spacing of stirrups, N is number of longitudinal bars, d_b is the diameter of longitudinal bars.

Bond stress distributions along the end anchorage in the support region were also determined analytically using a model for bond stress and slip in response to pullout forces shown in Fig. 4. End anchorage was assumed to be equivalent to a concrete rectangular prism with CFRP bar embedded in the centre of the concrete prism as shown in Fig. 4(a). The mathematical formulation of the response to pullout forces can be obtained by considering an infinitesimal length Δ_x of rectangular concrete prism. The slip, S_x, at a distance x along the reinforcement bar is defined as the relative displacement between the bar and concrete and can be expressed as:

$$S_x = u_{fx} - u_{cx} \tag{11}$$

The increment of the local slip dS within an infinitesimal bar length Δ_x at the location x can be found by differentiating Eq. (11),

$$\frac{dS_x}{dx} = \varepsilon_f - \varepsilon_c \tag{12}$$

where u_{fx} is displacement of the embedded reinforcement at point x, u_{cx} is displacement of the concrete at point x, ε_f and ε_c are reinforcement and concrete strains, respectively.

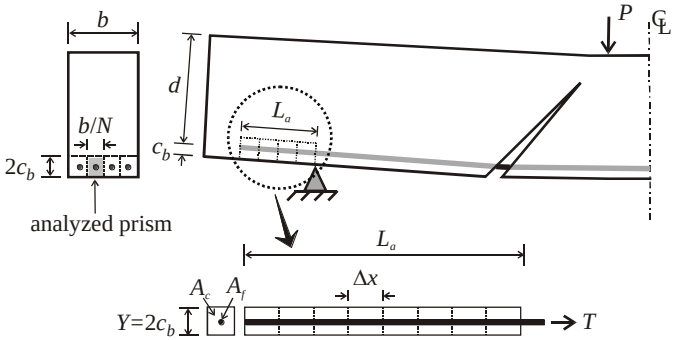

(a) Beam and the cross section with analyzed concrete rectangular prism.

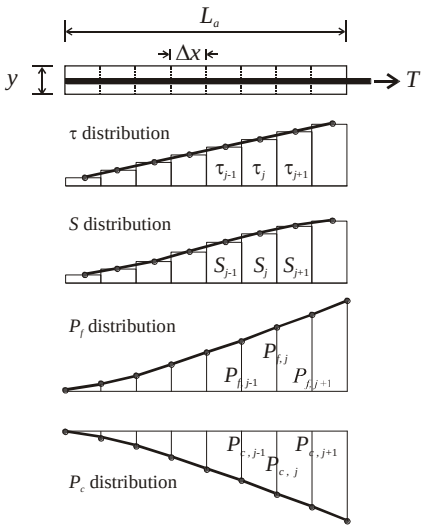

(b) The distribution of bond stress, slip, tensile force on CFRP bar and concrete along the prism.

Fig. 4. Pullout model for analytical study.

Applying the condition of equilibrium and compatibility of an infinitesimal length of the prism and differentiating Eq. (12) with respect to x, the second order differential equation governing the bond behavior along the embedment length of CFRP bar can be developed and expressed in Eq. (13).

$$\frac{d^2S_x}{dx^2} = \frac{(1+n\rho)}{A_f E_f}\phi\tau \tag{13}$$

where S_x is the local slip, $n = E_f/E_c$, $\rho = A_f/A_c$, τ is the local bond stress, and A_c is the area of concrete rectangular prism.

This equation indicates that modulus elasticity of concrete and embedded bar, area of rectangular concrete prism and embedded bar are parameters influenced the local bond stress-slip relationship. The distribution of bond stress, slip, tensile force carried by the CFRP bars and concrete along the concrete rectangular prism are illustrated in Fig. 4(b). The slip at each segment of the concrete rectangular prism shown in Fig. 4(b) can be solved numerically using Eq. (14).

$$S_j = S_{j-1} + \frac{1}{2}\Delta x\left(\frac{P_{f\,j-1} + P_{f\,j}}{A_f E_f} - \frac{P_{c\,j-1} + P_{c\,j}}{A_c E_c}\right) \tag{14}$$

The following equilibrium equation written in Eq. (15) must be satisfied for each assumed initial slip (load step) and given value of the tensile force, T, at the end of embedded bar:

$$P_{f,j} + P_{c,j} = P_{f,o} + P_{c,o} = T \tag{15}$$

If the equilibrium condition is not satisfied, the procedure should be repeated with a new value of assumed initial slip until Eq. (15) converges within a defined value of tolerance limit. On the other hand, if the equilibrium condition is satisfied, the computation process will be continued with the new value of the tensile force, T, and the distribution of slip, bond stress, P_f, and P_c can be plotted. The maximum tensile force of longitudinal reinforcement at the support obtained from the test, $T_{exp.}$, was used as the maximum tensile force, T, applied at the loaded end of embedded bar.

Furthermore, Eq's. (14) and (15) were solved numerically using a computer program developed by the author. The local bond stress–slip relationship used in this numerical analysis is shown in Fig. 5(a). This model was developed using experimental data from a pullout test carried out by Komiya et al. [17]. This pullout test used the same type of deformed CFRP bars produced by the same company as the bars used in this study. Hence, it is reasonable to use the data from that report in this study. In order to compare with the other pullout test data of the same bar type (deformed bar) and diameter, the data [17] were plotted together in Fig. 5(b) with the data obtained from the test carried out by Okelo, R. and Yuan, R. L [18]. It is shown from Fig. 5(b) that the maximum bond stress for deformed CFRP bars obtained from these two experimental data is about the same value. In addition, the ascending part of the curves show a good comparison between the two sets of experimental data.

A simple statistical procedure was carried out to fit the test results and the local bond stress-lip model for deformed CFRP bars as shown in the following equations is proposed. In this proposed equation, bond stress-slip model adopted from CEB/FIP Model Code [20] was simplified by assuming that the ascending and descending parts of the curve are linear.

$$0 < s \le s_1 \rightarrow \tau = 2.0\,\tau_{\max}\, s \tag{16}$$

$$s_1 < s \le s_2 \rightarrow \tau = \tau_{\max} + \left(s - s_1\right)\left[\left(\tau_f - \tau_{\max}\right)/\left(s_2 - s_1\right)\right] \tag{17}$$

$$s > s_2 \rightarrow \tau = \tau_f \tag{18}$$

$$\tau_{\max} = f_c^{'} s_1 \tag{19}$$

$$\tau_f = 0.2\tau_{\max} \tag{20}$$

where $s_1 = 0.5\,\text{mm}$ and $s_2 = 5\,\text{mm}$

Figure 5(a) also shows the comparison between Eligehausen, Popov, and Bertero (BPE) modified model [19] and the proposed model. It is shown that BPE modified model (ribbed bar type) has a lower bond strength. This result is reasonable because the value of maximum bond stress (τ_{max}) obtained from reference [19] is lower than the maximum bond stress in references [17] and [18] as that used to develop the proposed model.

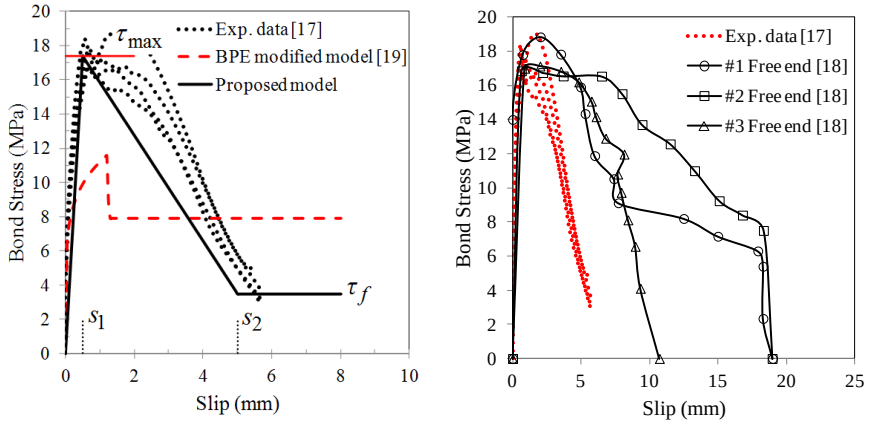

(a) Proposed model **(b) Experimental data [17, 18]**

Fig. 5. Proposed local bond stress–slip relationship used in analytical study.

4. Test Results and Discussion

4.1. Failure modes of the beams

Table 2 shows the theoretical and the experimental values of beam capacities. The types of failure for each beam are also listed in Table 2. Three types of failure mode were observed, i.e., bond splitting failure indicated by the occurrence of splitting cracks developing toward the support, shear failure indicated by concrete crushing in the loading point zone (shear compression), and flexural failure indicated by concrete crushing (in the top of concrete compression zone). Flexural failure occurred while the tensile stress of CFRP reinforcement was in the elastic state. Bond splitting failure mode was universally observed in beams with short end anchorage length (L_a = 25 mm). While, the failure modes of beams with L_a = 105 mm and 210 mm were bond, shear, or flexural failure, depending on the stirrup ratios, ρ_s, used in each of the beam.

Table 2. Theoretical and experimental values of beams capacities.

Beams	L_a	ρ_s	$\tau_{exp.}$	$T_{exp.}$	$V_{c\ theoretical}$					V_s	τ_{co}	τ_{st}	τ_u	V_{flex}	V_{bond}	V_{shear}	$V_{c\ exp.}$	$V_{exp.}$	Type of failure
					Eq.(1)	Eq.(2)	Eq.(3)	Eq.(4)	Eq.(5)	Eq.(6)									
	(mm)	(%)	(MPa)	(kN)	(kN)	(kN)	(kN)	(kN)	(kN)	(kN)	(MPa)	(MPa)	(MPa)	(kN)	(kN)	(kN)	(kN)	(kN)	
B-1		1.09	6.1	20.3						244.3	2.51	1.96	4.5		109.5	265.9	44.1	89.5	Bond
B-2	25	0.72	4.7	15.8						162.9	2.51	1.31	3.8		93.4	184.4	43.0	78.0	Bond
B-3	———	0.48	5.5	18.2						108.6	2.51	0.87	3.4		82.8	130.1	35.0	65.5	Bond
B-4		1.09	4.6	64.2						244.3	2.51	1.96	4.5		109.5	265.9	38.1	107.5	Flexural
B-5	105	0.72	4.3	60.8	42.5	41.6	24	29.9	21.5	162.9	2.51	1.31	3.8	130.5	93.4	184.4	37.1	102.1	Shear
B-6	———	0.48	4.4	61.6						108.6	2.51	0.87	3.4		82.8	130.1	35.6	90.0	Bond
B-7		1.09	2.9	80.7						244.3	2.51	1.96	4.5		109.5	265.9	50.6	118.0	Flexural
B-8	210	0.72	2.6	72.8						162.9	2.51	1.31	3.8		93.4	184.4	46.2	113.6	Flexural
B-9		0.48	3.0	84.4						108.6	2.51	0.87	3.4		82.8	130.1	40.1	106.0	Shear

Crack patterns of the beams at failure are illustrated in Fig. 6. It shows that the first flexural crack is initially developed in the constant moment zone (between two point loads). As the load increases, the cracks appear in the shear span zone followed by the occurrence of the diagonal shear cracks. Propagation of the diagonal crack is basically due to a condition of pure shear which occurs at the neutral axis and causes rotation of the principal stress trajectories. In the case of beams with insufficient end anchorage length (B-1, B-2, and B-3), the diagonal crack in the shear span zone was followed by bond-splitting cracks developing toward the support zone. This condition decreases bond strength in the support zone and caused failure in bond-splitting mode. In addition, the stirrup ratio significantly affect not only the capacity but also the crack patterns of the beams in the shear span zone as shown in Fig. 6.

4.2. Shear capacity of the beams

Shear force-deflection curves indicating beam capacities are shown in Fig. 7. The deflections plotted in this figure were obtained from data measured by LVDT located in the midspan of the beams. It is shown from Fig. 7 that beams with longer end anchorage length and higher stirrup ratio fail at higher shear forces and larger deflections. In addition, stiffness of the beams with higher stirrup ratio (B-4 and B-7) is slightly higher than stiffness of beams with lower (B-3, B-6 and B-9) stirrup ratio. Figure 7 also shows that all of the curves drop down rapidly without showing ductile behavior after reaching the peak load even though the beam failed in flexural mode which was indicated by concrete crushing at the top of concrete compression zone.

In this study, the total shear capacity of the beams was evaluated theoretically using empirical equations listed in Table 1 and Eq. (6). The results are shown in Table 2, it is shown that concrete shear capacity, V_c, calculated using Eq. (3) and Eq. (5) considerably underestimates the results obtained from the test and appears to be conservative for all beams examined in this study. While predicted values using Eq. (2) seem to be the closest to the appearance of experimental diagonal cracks, $V_{c\ exp.}$. It is also shown from Table 2 that the contribution of stirrups to shear capacity of the beams, V_s, is relatively high, even in the case of beams with the lowest stirrup ratio. This might be due to the high value of stirrups yield stress. However, not all of the calculated shear capacities, V_{shear}, of the beams were higher than calculated flexural capacities, V_{flex}, as listed in Table 2.

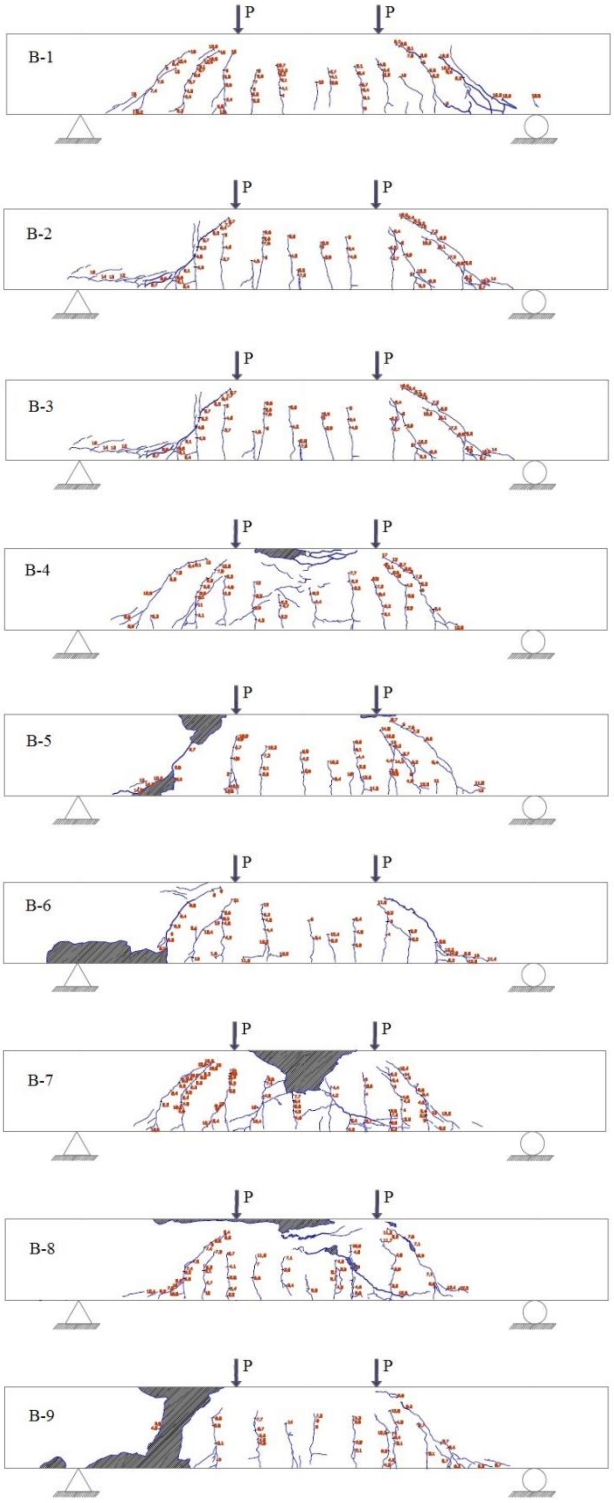

Fig. 6. Crack patterns of the beams at failure.

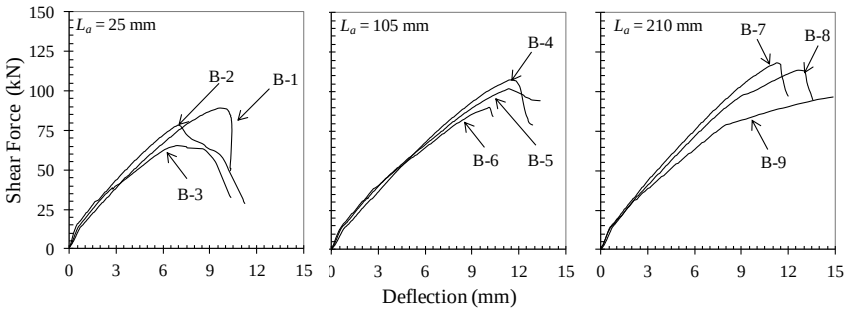

Fig. 7. Shear force-deflection curves of the beams.

4.3. Bond stress distributions along end anchorage

The calculated bond capacities for all of the beams , V_{bond}, were determined using Eq. (8) and by assuming that the lever arm of compression and tensile forces in the section is 0.875*d*. These values are lower than calculated shear capacities, V_{shear}, and calculated flexural capacities, V_{flex}, as listed in Table 2. In addition, the length of end anchorage is not considered in the calculation of V_{bond}. Hence, in order to ensure the bond strength, it is necessary to verify the bond distributions on end anchorage using a numerical model for bond stress and slip in response to pullout forces.

Figure 8 shows the predicted bond stress distributions along end anchorage calculated numerically using the numerical procedure described in the previous section. In this calculation the length of end anchorage was considered and a proposed bond stress-slip relationship shown in Fig. 5 was applied. In Fig 8, horizontal axis represents the position of the predicted bond stress along concrete rectangular prism (the distance from free end to the left support of the beam). While the vertical axis represents the predicted bond stress distributions at the maximum level of experimental tensile force at the support obtained from the test, T_{exp}. listed in Table 1.

It is also shown from Fig. 8 that bond stress exhibits a uniform distribution with very high values in case of end anchorage with short length (L_a = 25 mm). The high value of bond stress in short end anchorage indicates pullout failure due to insufficient bond length. Meanwhile, the predicted bond stress distributions along end anchorage with longer length (L_a = 105 mm and 210 mm) vary along the bond length and show smaller and more realistic values of bond stress especially at the end part of the concrete prism. In addition, the value of bond stresses along the concrete prism increases significantly toward the loaded end. This indicates that pullout failure is not taking place in the concrete prism with sufficient bond length as in fact observed in tested beams with sufficient end anchorage length.

The average bond stress, $\tau_{exp.}$, along end anchorage calculated using Eq. (7), and the value of theoretical bond strength, τ_u, calculated using Eq. (8) are plotted in Fig. 8 in comparison with analytical results. It is shown from this comparison that bond capacities calculated using Eq. (8), which does not take into account the length of end anchorage, show values closely comparable to the test results.

Figure 8 also demonstrates that the experimental bond stresses as well as predicted bond stress distributions in short end anchorage are higher than bond stresses in the longer ones.

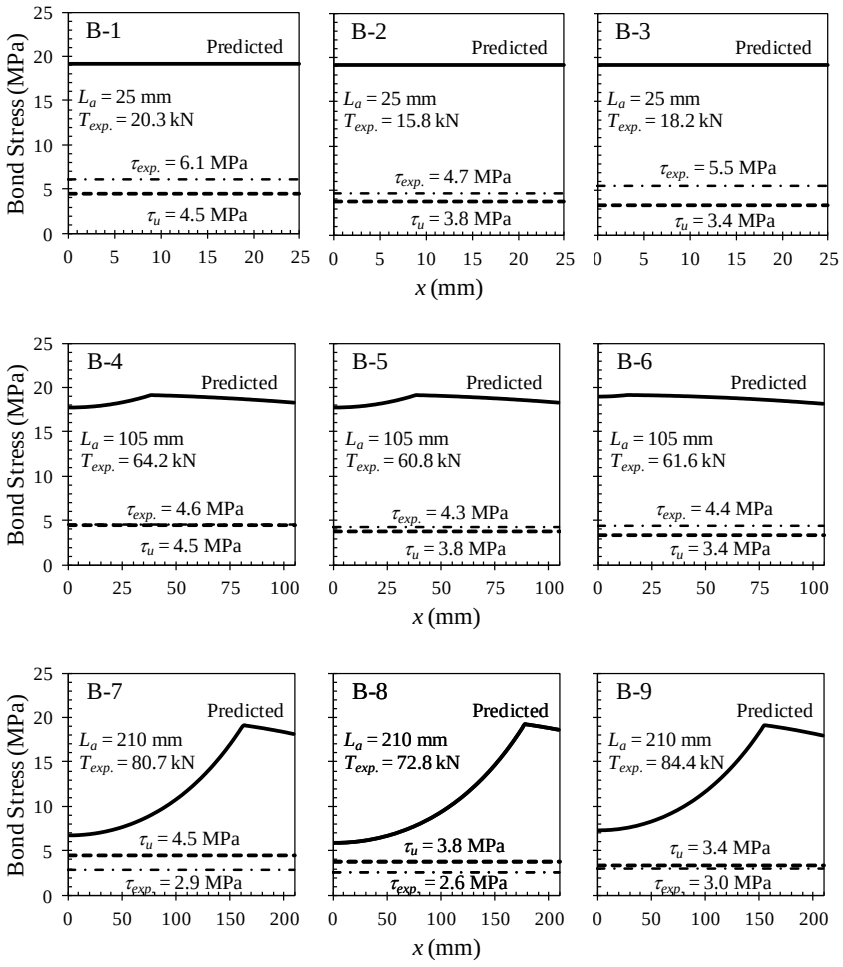

Fig. 8. Predicted and experimental bond stress distribution along end anchorage.

4.4. The behavior of tensile force acting on stirrups

Figure 9 shows the tensile forces acting on stirrups against the shear force for all of the beams. The vertical dash line points out the position of the theoretical value of concrete shear capacity, V_c, was calculated using Eq. (5). This Eq. (5) was selected as representative of the international codes for the design of structural concrete reinforced with FRP bars. Among the theoretical values of V_c calculated using theoretical equations listed in Table 2, Eq. (5) provides a value for V_c nearest to the point where tensile force on stirrups is observed to significantly increase as shown in Fig. 9.

It is shown from Fig. 9 that the tensile force acting on stirrups in case of beams with higher stirrup ratio is smaller than that in beams with lower stirrup ratio. It also demonstrates in beams B-6 (ρ_s = 0.48%), B-8 (ρ_s = 0.72%), and B-9 (ρ_s = 0.48%), that the tensile forces on stirrups on diagonal shear cracks, exceed the yield tensile force, T_{sy}, of stirrups. However, it is shown that none of the tensile forces on the stirrups exceed the yield force in case of beams with ρ_s = 1.09% even though the beams have sufficient end anchorage length.

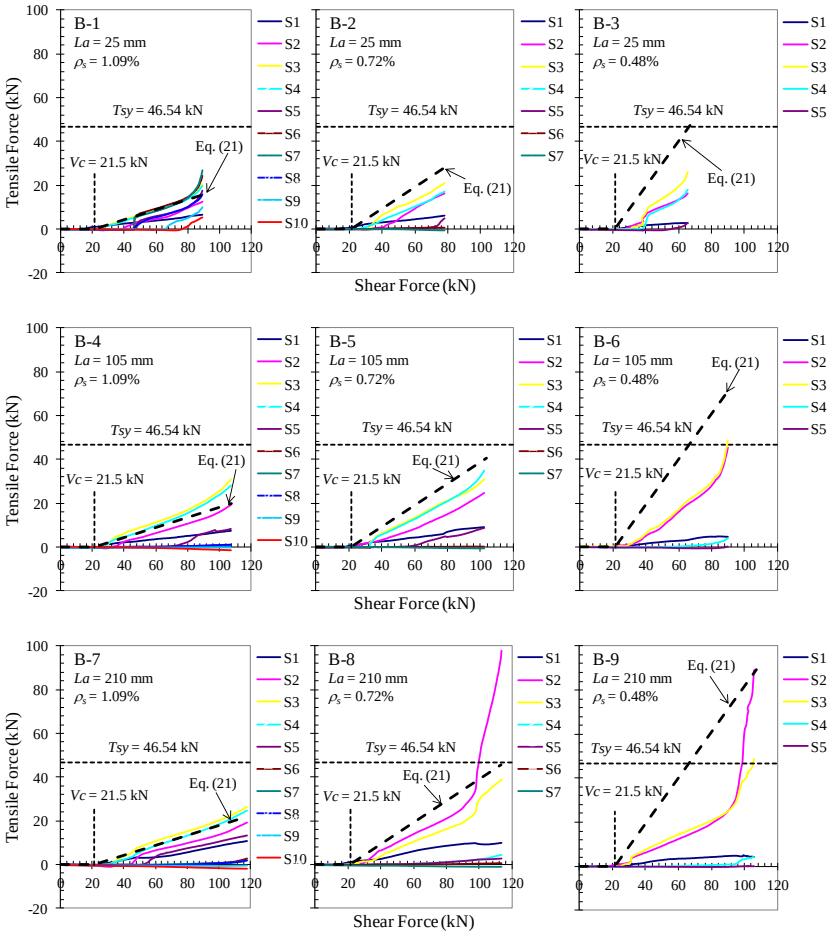

Fig. 9. Tensile forces acting on stirrups plotted against shear force.

The maximum values of tensile force obtained from the curves shown in Fig. 9 are plotted in Fig. 10 and Fig. 11. In these figures, the horizontal axis represents the location of stirrups measured from the left support, x, normalized by the effective depth, d, while the vertical axis represents the maximum tensile force, T_s, normalized by the value of yield force of the stirrups, T_{sy}. In case of T_s equal or greater than T_{sy}, the tensile force T_s is consider as T_{sy} hence the normalized value has a value of one. The effect of stirrup ratio on the tensile force of stirrups in the shear span zone is plotted in Fig. 10. As shown in Fig. 10, the highest tensile

forces on the stirrups are located in the middle of the shear span zone with the distance almost equal to the effective depth measured from the support.

Besides, it was also observed from the test that the location of the diagonal shear crack was similar to the location of the stirrups with the highest tensile force. This fact reveals that the stirrups carry the shear forces in the shear span zone especially after the occurrence of the diagonal cracks. In addition, the amount of tensile force acting on stirrups along the shear span length also depends on the position of the stirrups.

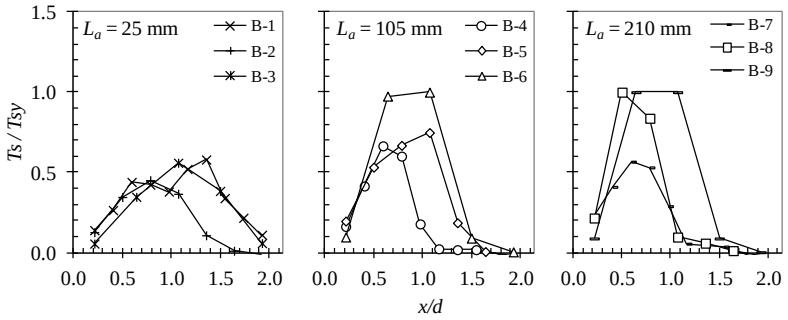

Fig. 10. Effect of stirrup ratio on the tensile force of stirrups.

Moreover, the effect of end anchorage length on the tensile force of stirrups in the shear span zone is shown in Fig. 11. It is shown that the tensile forces on stirrups in beams with L_a = 25 mm is smaller than that in beams with longer end anchorage length (L_a = 105 mm and 210 mm). This fact demonstrates that the beams with shorter end anchorage length have smaller load capacity than beams with longer end anchorage length. That is, as the end anchorage length increases the load capacity of the beam increases and the tensile force acting on the stirrups increases due to higher shear force acting in the shear span zone.

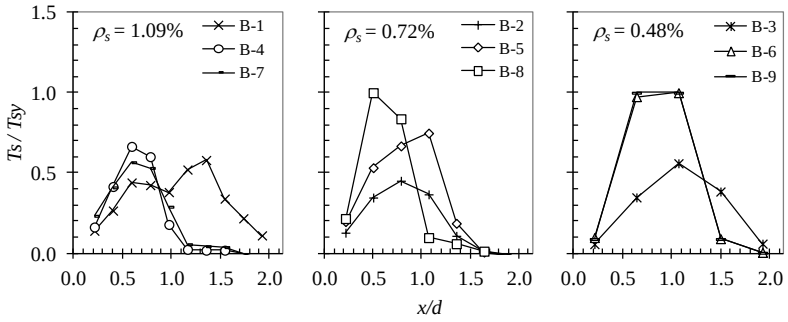

Fig. 11. Effect of end anchorage length on the tensile force of stirrups.

4.5. Proposed tensile force model of stirrups

Based on the experimental data described in the previous sections the author considers that the tensile force on stirrups is mainly affected by the shear force, the stirrup ratio, and number of stirrups along the shear span zone. Hence, it is rational to express the tensile force of stirrups as the function of shear force, *V*,

and concrete shear capacity, V_c. The process to determine the tensile force model of stirrups can be described schematically using Fig. 12 and the assumptions below. Selected data from experimental results of stirrups with maximum tensile force were collected and plotted as shown in Fig. 12. It is shown from this figure that the tensile force in stirrups increases significantly after the occurrence of diagonal shear crack represented by concrete shear strength, V_c. Hence only the data of $V > V_c$ were used to obtain the relationship between tensile force and shear force. Furthermore, linear regression (presented by bold dash line) has been applied to determine the relationship between shear force and the tensile force of stirrups. Finally, a simple model to predict the maximum tensile force of stirrups presented in Eq. (21) was obtained from statistical analysis.

$$T_S = \begin{cases} 0 & \text{if } V \le V_C \\ \omega(V - V_C) & \text{if } V > V_C \end{cases} \tag{21}$$

The concrete shear capacity, V_c, expressed in Eq. (21) is calculated using Eq. (5) while the process to determine the value of parameter ω can be described as follows. The authors believe that the effect of stirrup ratio, ρ_s, and number of stirrups along the shear span zone, N_s, can be written as

$$\omega = \alpha / N_S \rho_S \tag{22}$$

Figure 12 is created in order to examine the validity of Eq. (22). In this figure, the value of $T/(V\text{-}V_c)$ is plotted against the value of ω. The value of α in Eq. (22) was then adjusted using simple statistical procedure to fit the test data and to produce Eq. (23).

$$\omega = 2.5 / N_S \rho_S \tag{23}$$

It is noted from Eq. (21) that T_s equals zero if shear force smaller than V_c. The predicted tensile forces of stirrups calculated using Eq. (21) for each beams are plotted together with the test result and shown in Fig. 9 (presented by bold dash line). As an example, the detail of predicted tensile force on stirrups compared with the representative experimental data obtained from stirrup S2 in beam B-9 is shown in Fig. 13.

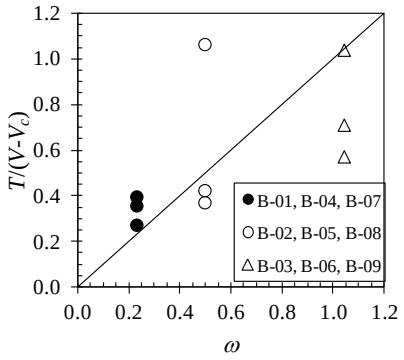

Fig. 12. The process to determine the effect of N_s and ρ_s.

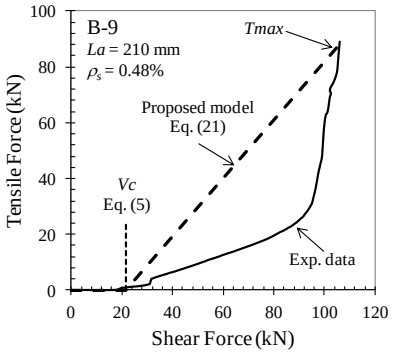

Fig. 13. Comparison between proposed model and selected data.

In practical application, the value of maximum tensile force, T_{max}, shown in Fig. 13 is obtained by substituting the minimum shear capacity value of $V_{flex.}$, V_{bond}, or V_{shear}, i.e., the shear force calculated from flexural, bond, or shear capacity, respectively. It is shown from Fig. 9 and Fig. 13 that, in case of beams with higher stirrup ratio, the proposed model predicts the maximum tensile force with a good level of accuracy. While, in the case of beams with lower stirrup ratio, the predicted values lie above observed values obtained from the test. This results indicates that the proposed model conservatively predicts the tension force acted on stirrups especially in case of beams with lower stirrup ratio.

Furthermore, selected experimental results from literature [21] summarized in Table 3 were used to validate the proposed model. The comparison between the test results and proposed model are shown in Fig. 14. The concrete shear capacity, $V_{c\ exp}$, shown in Table 3 was obtained by using the shear versus stirrups strain data. In addition the values of maximum shear force used in this validation were assumed as the minimum shear capacity value of $V_{flex.}$, V_{bond}, or V_{shear}.

Table 3. Selected additional data from literature [21].

Beams	f_c'	b	d	a/d	Longitudinal Reinf. Comp. ρ'	Comp. f_y	Tension ρ_w	Tension f_y	Stirrups s	Stirrups ρ_s	Stirrups f_y	$V_{c\ ACI}$ Eq.(4)	$V_{s\ ACI}$ Eq.(6)	V_{flex}	V_{bond}	V_{shear}	$V_{c\ exp.}$	N_s	ω
	(MPa)	(mm)	(mm)		(%)	(MPa)	(%)	(MPa)	(mm)	(%)	(MPa)	(kN)	(kN)	(kN)	(kN)	(kN)	(kN)		
G1-C60	32.5	610	635	3.1	0.3	415	1.56	415	203	0.11	415	386.2	183.9	711.2	874.1	570.1	289.0	9.0	2.4
G1-M80	32.5	610	635	3.1	0.3	694	1.04	694	254	0.09	552	375.2	195.6	812.8	828.1	570.8	231.0	8.0	3.4
G1-M10(	34.0	610	635	3.1	0.3	694	1.04	694	330	0.07	694	383.2	189.2	812.8	834.6	572.4	298.0	6.0	5.9

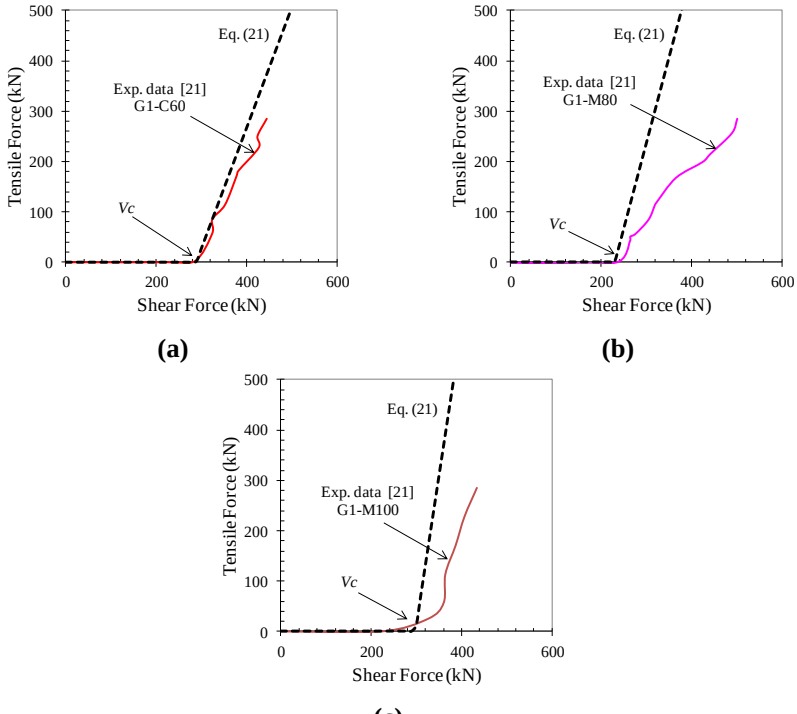

Fig. 14. Comparison between proposed model and experimental data [21].

The tensile forces of stirrups plotted in Fig. 14 were obtained using the data listed in Table 3 and the shear versus stirrups strain records [21]. It is shown from Fig. 13 that Eq. (21) predicts conservatively the growth of tensile force on stirrups. Figures 14(b) and (c) show that the maximum tensile forces of the proposed model are about 40% to 50% higher than the test results. It might be due to the termination of loading before the stirrups reach the predicted maximum tensile force.

5. Conclusions

The test data from nine concrete beams reinforced with CFRP bars were used in order to study the effect of end anchorage length and stirrup ratio on bond and shear behavior. Based on the test results and numerical calculation, the behavior of bond stress distributions along the end anchorage was analyzed. Consequently, a tension force model of stirrups as a function of shear force, V, concrete shear capacity, V_c, stirrup ratio, ρ_s, and number of stirrups along the shear span zone, N_s. was proposed. Finally, the following conclusions are drawn:

- Beams with higher stirrup ratio fail at higher shear forces and larger deflections. The stiffness of the beams with higher stirrup ratio is slightly higher than beams with lower stirrup ratio. In addition, the stirrup ratio affects significantly the failure type of the beams.
- End anchorage beyond the support has an important role in improving the bond capacity of the beams. The beams with insufficient length of end anchorage failed in bond-splitting failure mode due to premature bond loss at the support zone indicated by the occurrence of bond splitting cracks developing toward the support, while beams with sufficient end anchorage length failed in flexure or shear mode depending on the number of stirrups.
- The load carrying capacity of the concrete beams reinforced with CFRP bars drops rapidly without showing ductile behavior after reaching the peak load even though the beam failed in flexural mode.
- The shear capacity of the concrete, V_c, required in ACI 440.1R-06 underestimates the values of concrete shear capacity, $V_{cexp.}$, obtained from the test and appears to be conservative for design application.
- Bond strength calculated using Eq. (8) predicts bond capacity of the beams with reasonable accuracy although this empirical equation was originally generated from concrete section reinforced with steel bars,
- Predicted bond stress distributions along the concrete rectangular prism using numerical procedure shows a uniform distribution of bond stresses along insufficient end anchorage with very high values. Meanwhile more reasonable profiles of bond stress distributions along end anchorage are shown in case of adequate end anchorage length.
- The stirrups in the location of diagonal cracks show high tensile force with the distance measured from the support almost equal to the effective depth. The beams with lower stirrup ratio show higher tensile force on stirrups.
- In case of beams with lower stirrup ratio, observed values of tensile forces lie below the predicted value. While, in the case of beams with higher stirrup

ratio, the proposed model predicts the maximum tensile force with a good level of accuracy.

References

1. Bresler, B. (1974). *Reinforced concrete engineering, Vol. I, Materials, structural elements, safety*. John Wiley and Sons, New York.
2. Magnusson, J. (2000). *Bond and anchorage of ribbed bars in high-strength concrete*. PhD Thesis. Division of Concrete Structures, Chalmers University of Technology, Göteborg, Sweden.
3. Thamrin, R.; and Kaku, T. (2005). Development length evaluation of reinforced concrete beam with CFRP bars. *Proceedings of International Symposium on Bond Behaviour of FRP in Structures*, Hongkong, China, 393-399.
4. Mylrea, T.D. (1948). Bond and anchorage. *ACI Journal*, 44(3), 521-552.
5. Pay, A.C.; Canbay, E.; and Frosch, F.J. (2014). Bond strength of spliced fiber-reinforced polymer reinforcement. *ACI Structural Journal*, 111(2), 257-266.
6. Azlina, N.; Ibrahim, A.; Thamrin, R.; and Hamid, H.A. (2013). Experimental investigation on the shear behaviour of concrete beams reinforced with GFRP reinforcement bars. *Journal of Advanced Materials Research*, 626, 559-563.
7. Azlina, N.; Thamrin, R.; and Ibrahim, A. (2013). Shear capacity of non-metallic (FRP) reinforced concrete beams with stirrups. *International Journal of Engineering and Technology*, 5(5), 593-598.
8. Azlina, N.; Thamrin, R.; Ibrahim, A.; and Hamid, H.A. (2014). Strain distribution on reinforcement of concrete beams reinforced with glass fiber reinforced polymer (GFRP) bars. *International Journal of Key Engineering Materials*, 594-595, 812-817.
9. ACI 318M-08. (2008). *Building code requirements for structural concrete and commentary*, American Concrete Institute.
10. ACI 440.1R-06. (2006). *Guide for the design and construction of structural concrete reinforced with FRP bars*, American Concrete Institute.
11. Thamrin, R.; and Kaku, T. (2007). Bond behavior of CFRP bars in simply supported reinforced concrete beam with hanging region. *Journal of Composites for Construction, ASCE*, 11(2), 129-137.
12. Morita, S.; and Fujii, S. (1982), Bond capacity of deformed bars due to splitting of surrounding concrete. *Bond in Concrete*, Applied Science Publisher, 331-341.
13. Plizzari, G.A.; Deldossi, M.A.; and Massimo, S. (1998). Transverse reinforcement effects on anchored deformed bars. *Magazine of Concrete Research*, 50(2), 161-177.
14. Zsutty, T.C. (1968). Beam shear strength prediction by analysis of existing data. *ACI Journal*, 65(11), 942–951.
15. Niwa, J.; Yamada, K.; Yokozawa, K.; and Okamura, H. (1987). Revaluation of the equation for shear strength of reinforced concrete beams without web reinforcement. *Concrete Library International of JSCE*, (9), 65-84.
16. British Standards Institution. (2014). *Eurocode 2: Design of concrete structures - Part 1-1: General rules and rules for buildings.* BSI, London, UK.

17. Komiya, I.; Kaku, T.; and Kutsuna, H. (1999). Bond characteristic of FRP rods No. 3. *Proceedings of AIJ Annual Conference*, Japan, 623–624 (in Japanese).
18. Okelo, R.; and Yuan, R. L. (2005). Bond strength of fibre reinforced polymer rebars in normal strength concrete. *Journal of Composites for Construction, ASCE*, 9(3), 203-213.
19. Cosenza, E.; Manfredi, G.; and Realfonzo, R. (1997). Behavior and modelling of bond of FRP rebars to concrete. *Journal of Composites for Construction, ASCE*, 1(2), 40-51.
20. CEB/FIP Model Code, (1990). - Final Draft. *Information bulletin 204, Comite Euro- International du Beton*, Lausanne, Switzerland.
21. Munikrishna, A.; Hosny, A.; Rizkalla, S.; and Zia, P. (2011). Behavior of concrete beams reinforced with ASTM A1035 grade 100 stirrups under shear. *ACI Structural Journal*, 108(1), 34-41.